LETTER

doi:10.1038/nature13713

Discovery and characterization of small molecules that target the GTPase Ral

Chao Yan[1], Degang Liu[2], Liwei Li[2], Michael F. Wempe[3], Sunny Guin[1], May Khanna[2], Jeremy Meier[4], Brenton Hoffman[4], Charles Owens[1], Christina L. Wysoczynski[5], Matthew D. Nitz[6], William E. Knabe[2], Mansoor Ahmed[7,8], David L. Brautigan[6], Bryce M. Paschal[9], Martin A. Schwartz[7,8], David N. M. Jones[5], David Ross[3], Samy O. Meroueh[2,10] & Dan Theodorescu[1,5,11]

The Ras-like GTPases RalA and RalB are important drivers of tumour growth and metastasis[1]. Chemicals that block Ral function would be valuable as research tools and for cancer therapeutics. Here we used protein structure analysis and virtual screening to identify drug-like molecules that bind to a site on the GDP-bound form of Ral. The compounds RBC6, RBC8 and RBC10 inhibited the binding of Ral to its effector RALBP1, as well as inhibiting Ral-mediated cell spreading of murine embryonic fibroblasts and anchorage-independent growth of human cancer cell lines. The binding of the RBC8 derivative BQU57 to RalB was confirmed by isothermal titration calorimetry, surface plasmon resonance and ^{1}H–^{15}N transverse relaxation-optimized spectroscopy (TROSY) NMR spectroscopy. RBC8 and BQU57 show selectivity for Ral relative to the GTPases Ras and RhoA and inhibit tumour xenograft growth to a similar extent to the depletion of Ral using RNA interference. Our results show the utility of structure-based discovery for the development of therapeutics for Ral-dependent cancers.

More than one-third of human tumours harbour activating *RAS* mutations[2], which has motivated extensive efforts to develop inhibitors of Ras for cancer therapy. However, therapies directed at interfering with post-translational modifications of Ras[3] had poor clinical performance; therefore, efforts shifted to targeting the signalling components downstream of Ras such as the Raf–MEK–ERK mitogen-activated protein kinase pathway[4] and the phosphatidylinositol-3-OH kinase–AKT–mTOR pathway[5]. A third pathway downstream of Ras leads to the activation of the Ras-like small GTPases RalA and RalB[6], and this pathway has not been targeted to date. Active Ral activates cellular processes through effectors, including Ral-binding protein 1 (RALBP1; also known as RLIP76 and RIP1)[7], the human exocyst subunits SEC5 and EXO84, filamin and phospholipase D1 (refs 8–10). These effectors mediate regulation of cell adhesion (anchorage independence), membrane trafficking (exocytosis and endocytosis), mitochondrial fission, and transcription. RalA and RalB are important drivers of the proliferation, survival and metastasis of multiple human cancers, including skin[11], lung[12], pancreatic[1], colon[13], prostate[14], and bladder[15,16] cancers.

We set out to discover small molecules that inhibit the intracellular actions of the Ral-family GTPases. Our approach was based on the hypothesis that molecules that selectively bind to Ral–GDP might restrict Ral to an inactive state in the cell, making it unavailable to promote processes linked to tumorigenesis. Comparing the available three-dimensional structures of RalA revealed differences in a region adjacent to, but distinct from, the guanine nucleotide binding pocket (Fig. 1). This site is formed by the switch-II region (amino acids 70–77), the α2 helix (amino acids 78–85) and one face of the α3 helix (Fig. 1a). Its proximity to the previously described C3bot binding site[17] supports the notion that small molecule occupancy at this site could inhibit function. The crystal structures used in the comparison included RalA–GDP (Protein Data Bank (PDB) ID, 2BOV; Fig. 1a, b) and RalA–GNP (RalA bound to a non-hydrolysable form of GTP, the GTP analogue GMP–PNP) in complex with EXO84 (PDB ID, 1ZC4; Fig. 1c) or SEC5 (PDB ID, 1UAD, Fig. 1d). The volumes calculated for this binding site were 175 Å^3 for RalA–GDP (Fig. 1b), 155 Å^3 for RalA–GNP–EXO84 (Fig. 1c) and 116 Å^3 for RalA–GNP–SEC5 (Fig. 1d). To the best of our knowledge, a RalB–GDP crystal structure is not available. However, in the RalB–GNP structure (PDB ID, 2KE5; Extended Data Fig. 1), this binding site is largely absent. Next, we used a structure-based virtual screening approach[18] to identify small molecules that bind to this site in RalA–GDP by individually docking 500,000 compounds to this site (using ChemDiv, v2006.5)[19] and by scoring protein–ligand complexes based on calculated interaction energies. This process led to the selection of 88 compounds.

We developed an enzyme-linked immunosorbent assay (ELISA) for assaying Ral activity in living cells based on the selective binding of active RalA–GTP to its effector protein RALBP1. This assay used J82 human bladder cancer cells that stably expressed Flag-tagged RalA. The Flag epitope tag greatly increased the sensitivity and dynamic range of the assay compared with using Ral-specific antibodies for detection (Extended Data Fig. 2a). Cells were treated with each of the 88 compounds (tested at 50 μM), and then extracts were prepared. The binding of Flag–RalA to recombinant RALBP1 that had been immobilized in 96-well plates was quantified. In this assay, RalA binding reflects Ral's GTP loading and capacity for effector activation. The compounds RBC6, RBC8 and RBC10 (structures shown in Fig. 1e–g) reduced the activation of RalA in living cells (Fig. 1h), while compounds RBC5, RBC7 and RBC42 (structures not shown) had no effect and thus served as negative controls. None of the 88 compounds inhibited GTP or GDP binding to purified recombinant RalA (Supplementary Table 1), which is consistent with the interaction site being distinct from that used for binding guanine nucleotides.

Another cell-based assay was also used to assess the effects of these 88 compounds. Ral is required for lipid raft exocytosis and cell spreading on fibronectin-coated coverslips by murine embryonic fibroblasts (MEFs)[20]. The depletion of RalA with a specific short interfering RNA (siRNA) inhibited the spreading of wild-type MEFs, whereas caveolin-deficient ($Cav1^{-/-}$) MEFs retained the capacity to spread after RalA depletion. When the effects of RBC6, RBC8 and RBC10 on cell spreading in wild-type and $Cav1^{-/-}$ MEFs were tested, only the wild-type MEFs were inhibited (Fig. 1i and Extended Data Fig. 2b). RBC6 and RBC8 (but not RBC10) are related structures with the same bicyclic core (Fig. 1e–g); specific substitutions gave rise to similar but somewhat different binding orientations in the allosteric binding cavity (Extended Data Fig. 2c–e). We therefore focused on RBC6 and RBC8 in further experiments.

[1]Department of Surgery, University of Colorado, Aurora, Colorado 80045, USA. [2]Department of Biochemistry, Indiana University School of Medicine, Indianapolis, Indiana 46202, USA. [3]Department of Pharmaceutical Sciences, University of Colorado, Aurora, Colorado 80045, USA. [4]Cardiovascular Research Center, University of Virginia, Charlottesville, Virginia 22908, USA. [5]Department of Pharmacology, University of Colorado, Aurora, Colorado 80045, USA. [6]Department of Microbiology, Immunology, and Cancer Biology, University of Virginia, Charlottesville, Virginia 22908, USA. [7]Department of Cardiology, Yale University, New Haven, Connecticut 06511, USA. [8]Department of Cell Biology, Yale University, New Haven, Connecticut 06511, USA. [9]Department of Biochemistry and Molecular Genetics, University of Virginia, Charlottesville, Virginia 22908, USA. [10]Department of Chemistry and Chemical Biology, Indiana University – Purdue University, Indianapolis, Indiana 46202, USA. [11]University of Colorado Comprehensive Cancer Center, Aurora, Colorado 80045, USA.

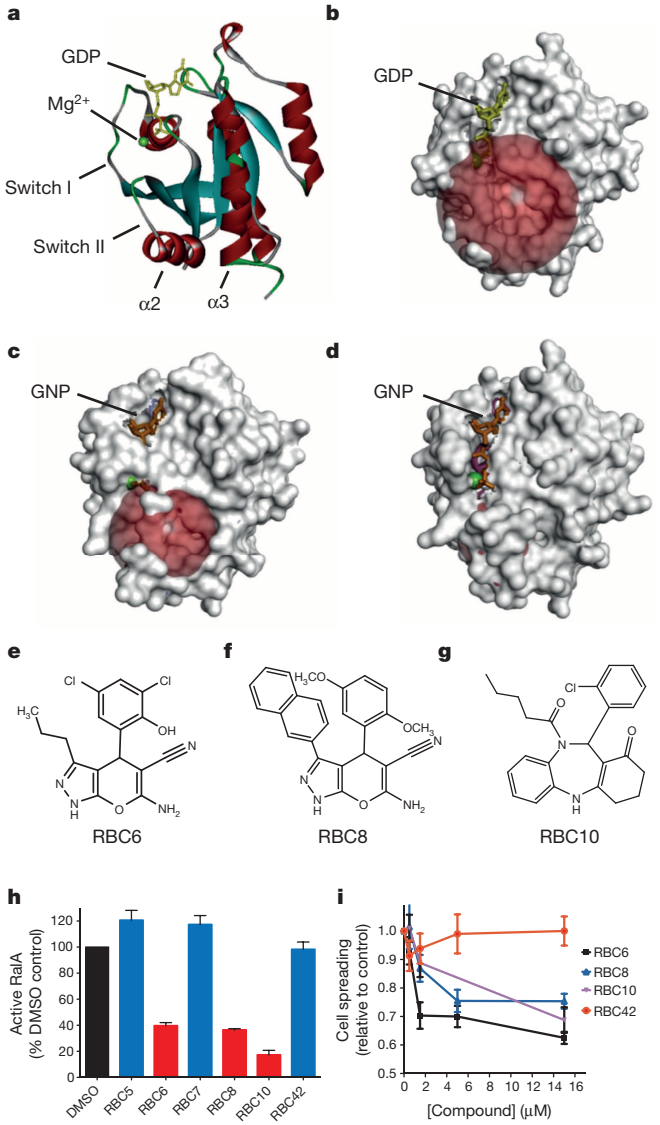

Figure 1 | Structure-based *in silico* library screening and cell-based secondary screening identified RBC6, RBC8 and RBC10 as lead compounds for Ral inhibition. **a**, **b**, Structural model of RalA–GDP as a ribbon (**a**) or surface (**b**) representation. GDP is shown in yellow, Mg^{2+} is shown as a green sphere, α-helices are shown in red, and β-sheets are shown in cyan. The red sphere and surfaces indicate the water accessible area in the binding cavity. All models were generated with Accelrys Discovery Studio software using published structures. **c**, **d**, Surface representations of RalA–GNP in complex with EXO84 (EXO84 not shown) (**c**) and RalA–GNP in complex with SEC5 (SEC5 not shown) (**d**). **e**–**g**, Chemical structure of RBC6 (**e**), RBC8 (**f**) and RBC10 (**g**). **h**, RalA ELISA results for the top compounds (RBC6, RBC8 and RBC10) and for three ineffective compounds (RBC5, RBC7 and RBC42), as identified by computational screening. J82 cells overexpressing Flag–RalA were treated with each compound for 1 h and then subjected to a RalA ELISA, as described in Methods. Data are presented as the mean ± s.d. of three technical replicates and expressed as the percentage of DMSO control. **i**, Dose response effect of RBC6, RBC8 and RBC10 on the RalA-dependent spreading of wild-type MEFs. MEFs were treated with 0–15 μM each compound for 1 h and subjected to the MEF-spreading assay, as described in Methods. Data are presented as the mean ± s.d. of three technical replicates.

To test for the direct binding of compounds to Ral, we used ^{1}H–^{15}N TROSY NMR spectroscopy. The NMR structure of RalB in complex with GNP has been solved (PDB ID, 2KE5; Biological Magnetic Resonance Bank (BMRB) ID, 15230)[21]; therefore, we focused on this isoform. First, we obtained complete backbone NMR chemical shift assignments for the RalB–GDP complex (see Methods), and then we compared the ^{1}H–^{15}N-TROSY NMR spectrum of RalB–GDP and RalB–GNP to determine the chemical shift differences between the GTP-bound and GDP-bound states. Almost all of the differences were confined to residues that interact with the third phosphate of the GTP (Extended Data Fig. 3a, b). ^{1}H–^{15}N-TROSY spectra were then recorded in the presence of the compound RBC8 or dimethylsulphoxide (DMSO) as a control, and the chemical shift changes were compared. RBC8 induced chemical shift changes in RalB–GDP but not in RalB–GNP, indicating that RBC8 shows selectivity for the GDP-bound form of Ral (Extended Data Fig. 3c, d). Moreover, RBC5, which did not affect the level of active Ral in the cell-based ELISA assay, did not induce chemical shift changes in RalB–GDP (Extended Data Fig. 3e), thereby serving as an additional negative control.

On the basis of all of these data, including the structural features, a series of RBC8 derivatives was synthesized and tested for binding *in vitro*. We chose BQU57 for further evaluation because of its superior performance to RBC8 and its drug-like properties (Fig. 2a, Extended Data Fig. 4a and synthesis pathway in Supplementary Methods). A detailed NMR analysis of the binding between BQU57 and RalB–GDP was carried out. The NMR spectrum of RalB–GDP (100 μM) in the absence and presence of BQU57 (100 μM) is shown in Fig. 2b. Concentration-dependent chemical shift changes for representative residues are shown in Fig. 2c. A plot of the chemical shift changes with BQU57 (100 μM) as a function of sequence (Fig. 2d) shows that residues that exhibit marked changes are located in the switch-II (amino acids 70–77) and α2 helix (amino acids 78–85) regions. Because no RalB–GDP crystal structure is available, a homology model was generated based on similarity to RalA–GDP, and the residues that displayed chemical shift changes in response to the compounds were mapped onto this model (Fig. 2e). The majority of the chemical shift changes were localized to the allosteric site, consistent with assignment of BQU57 binding to this site based on modelling. Similar to the results for RBC8, BQU57 (100 μM) did not bind to RalB–GNP (100 μM) as indicated by the minimal chemical shift changes in the NMR spectrum (Extended Data Fig. 4b). Analysis of the NMR chemical shift titrations revealed that the binding of BQU57 was stoichiometric up to the apparent limiting solubility of the drug (which was estimated as ~100 μM in control experiments without protein) (Extended Data Fig. 4c). The binding of BQU57 to RalB–GDP was also determined, by using isothermal titration calorimetry (ITC), which yielded a dissociation constant (K_d) of 7.7 ± 0.6 μM (Fig. 2f). This finding was similar to the results from surface plasmon resonance (SPR), which gave a K_d of 4.7 ± 1.5 μM (Extended Data Fig. 4d).

Next we evaluated the action of RBC8, BQU57 and RBC5 (the last as a negative control) on the human lung cancer cell lines H2122, H358, H460 and Calu-6. Ral promotes anchorage independence[1,20]; therefore, we measured cell growth in soft agar. We examined drug uptake and found that RBC8, BQU57 and RBC5 were readily taken into cells (Extended Data Fig. 5a–c). In addition, we found that all four cell lines were sensitive to siRNA-mediated depletion of K-*RAS* (Extended Data Fig. 6a, b) but that only H2122 and H358 cells were sensitive to *RAL* knockdown (Extended Data Fig. 6c, d). We used this characteristic to assess the specificity of the compounds for inhibiting Ral. Colony formation in soft agar showed that the Ral-dependent lines H2122 and H358, but not H460 or Calu-6, were sensitive to treatment with RBC8 or BQU57 (Fig. 3a, b). The half-maximum inhibitory concentration (IC_{50}) of RBC8 was 3.5 μM in H2122 cells and 3.4 μM in H358 cells; for BQU57, the IC_{50} was 2.0 μM in H2122 cells and 1.3 μM in H358 cells. The inactive control compound RBC5 did not inhibit the growth of any of these cell lines (Extended Data Fig. 5d). Additionally, a Ral pull-down assay using RALBP1-bound agarose beads[8] showed that RBC8 and BQU57, but not RBC5, inhibited both RalA and RalB activation in both the H2122 and H358 cell lines (Extended Data Fig. 5e).

To further examine the specificity of these compounds for Ral, *RALA* and *RALB* were knocked down in H2122 and H358 cells with specific siRNAs. RBC8 or BQU57 treatment showed no further inhibition of colony formation after *RAL* knockdown (Fig. 3c–f and Extended Data Fig. 6e). This supports the conclusion that the inhibition of cell growth

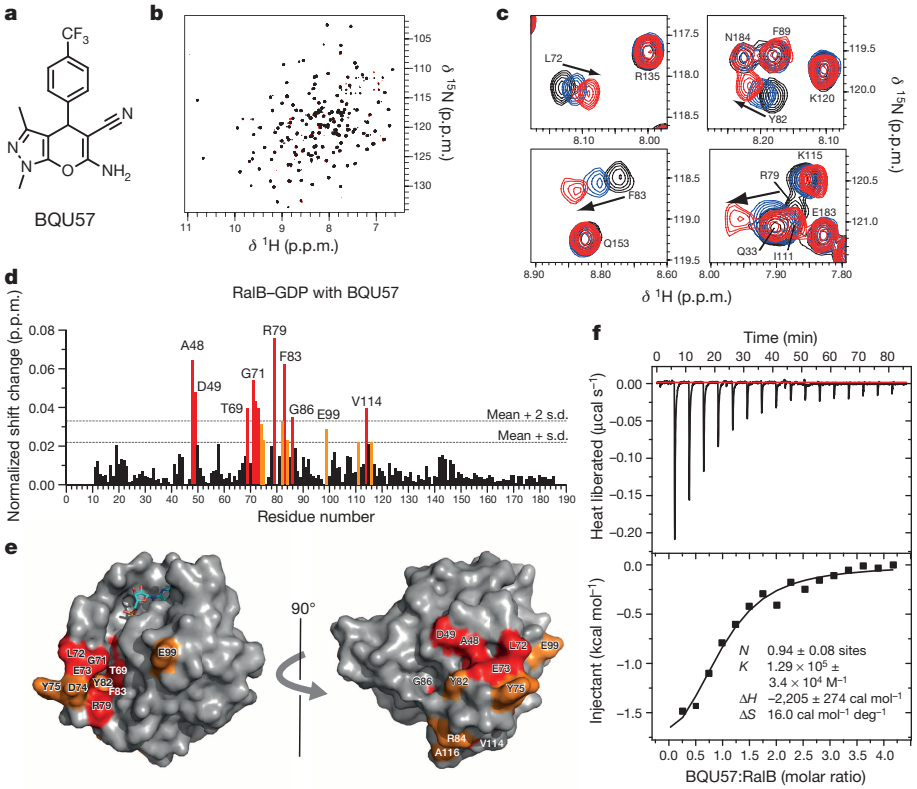

Figure 2 | Characterization of compounds binding to Ral. **a**, Chemical structure of BQU57. **b**, Overlay of the ^{15}N-TROSY spectrum of 100 μM RalB–GDP in the absence (black) and presence (magenta) of 100 μM BQU57. **c**, Selected residues of RalB–GDP in the absence (black) and presence (40 μM, blue; 100 μM, red) of increasing concentrations of BQU57. **d**, Plot of chemical shift changes as a function of residue number comparing RalB–GDP alone and in the presence of 100 μM BQU57 (coloured bars denote significant changes; red > mean + 2 s.d.; orange > mean + 1 s.d.). **e**, Residues showing significant chemical shift changes (colour coding as in **d**) mapped to their location on a homology model of the RalB–GDP complex generated from the published RalA–GDP structure (PDB ID, 1U90); GDP is shown as a stick representation. **f**, Determination of K_d for the binding of BQU57 to RalB–GDP using ITC to measure the heat liberated (μcal) as a function of time. The ITC data represent three independent experiments. ΔH, enthalpy; K, association constant; N, stoichiometry; ΔS, entropy.

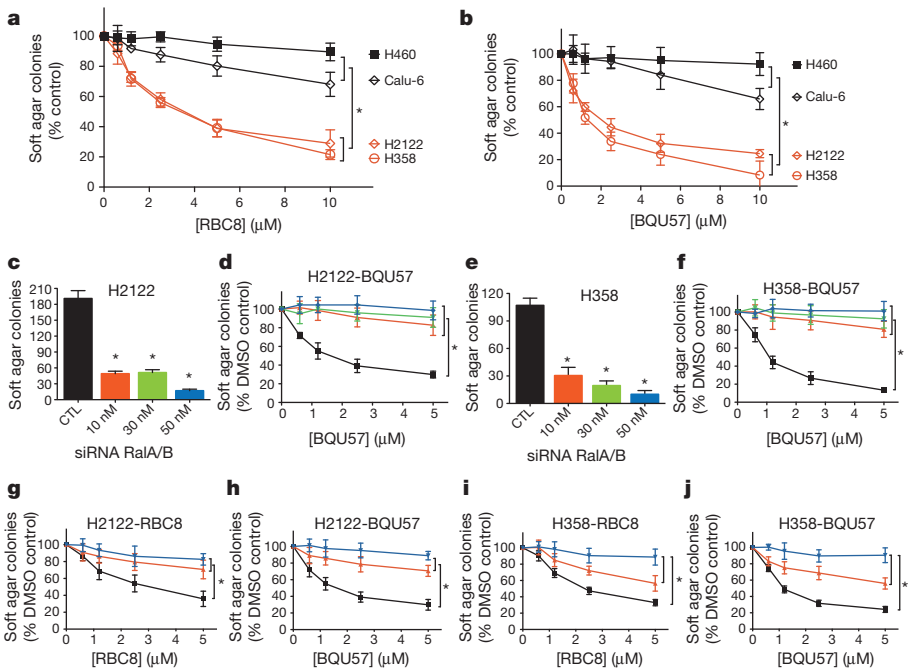

Figure 3 | Growth inhibitory activity of Ral inhibitors on human cancer cell lines. **a**, **b**, Effects of RBC8 (**a**) and BQU57 (**b**) treatment on the anchorage-independent growth of four human lung cancer cell lines. The cells were seeded in soft agar containing various concentrations of each compound, and colonies were counted after 2–4 weeks. Cell lines that are sensitive to *RAL*-directed knockdown (H2122 and H358) are shown in red, and cell lines that are resistant to *RAL*-directed knockdown (H460 and Calu-6) are shown in black. **c**–**f**, Effect of siRNA-mediated knockdown of both *RALA* and *RALB* (RalA/B) on drug-induced growth inhibition in soft agar of H2122 cells (**c**, **d**) and H358 cells (**e**, **f**). Cells were transfected with 10, 30 or 50 nM siRNA for 48 h, collected and subjected to the soft agar colony formation assay. The effect of siRNA alone on the soft agar colony number is shown in **c** (H2122) and **e** (H358); the effect of siRNA plus drug treatment on colony formation is shown as the percentage of the DMSO-treated control in **d** (H2122) and **f** (H358). The control is shown in black; 10 nM drug, in red; 30 nM drug, in green; and 50 nM drug, in blue. **g**–**j**, Effect of the overexpression of constitutively active RalA^{G23V} and RalB^{G23V} on drug-induced growth inhibition in soft agar of H2122 cells (**g**, **h**) and H358 cells (**i**, **j**). H2122 cells or H358 cells were transiently transfected with Flag alone (black), Flag–RalA^{G23V} (red) or Flag–RalB^{G23V} (blue) for 48 h before the soft agar colony formation assay. The results in all panels are presented as the mean ± s.d. of triplicate experiments. *, $P < 0.05$, Student's *t*-test or Dunnett's test.

by these compounds depends on Ral proteins. Moreover, overexpression of constitutively active (GTP-bound form[22]) $RalA^{G23V}$ or $RalB^{G23V}$ mutant proteins (Extended Data Fig. 6f), which do not bind to these compounds (Extended Data Figs 3d and 4b), mitigated the inhibition of H2122 and H358 cell growth by these compounds (Fig. 3g–j and Extended Data Fig. 6f). Together, these data provide evidence that RBC8 and BQU57 act specifically through the GDP-bound form of Ral proteins.

The inhibition of Ral activity and tumour growth by these compounds were evaluated in human lung cancer xenografts in mice. The pharmacokinetics of RBC8 and BQU57 were analysed in mice. Serum concentrations were determined using liquid chromatography coupled to tandem mass spectrometry (LC-MS/MS) after intraperitoneal injection of the compound. RBC8 and BQU57 showed properties that define good drug candidates (Extended Data Fig. 7a). We then determined compound entry to tumour tissue 3 h after dosing, and the compounds were detected in tumour tissue *in vivo* (Extended Data Fig. 7b, c). To test the effect of Ral inhibitors on tumour xenograft growth, nude mice were inoculated subcutaneously with H2122 (human) cells and treated intraperitoneally with 50 mg per kg body weight of RBC8 per day for 21 days (except on weekends). RBC8 inhibited tumour growth (Fig. 4a and Extended Data Fig. 7d) to a similar extent to dual knockdown of *RALA* and *RALB* (Fig. 4b). Another lung cancer line, H358, yielded similar results (Extended Data Fig. 7e). BQU57 was tested *in vivo* at several different doses (10, 20 and 50 mg per kg body weight per day), and dose-dependent growth inhibition effects were observed (Fig. 4c).

To further evaluate the specificity of the compounds for the Ral-family GTPases, H2122 tumour xenografts (median size, 250 mm^3) were collected 3 h after a single intraperitoneal injection of RBC5 (50 mg per kg body weight), RBC8 (50 mg per kg body weight) or BQU57 (10, 20 and 50 mg per kg body weight), and the activation of Ral in tumour extracts was analysed in RALBP1 pull-down assays. Both RalA and RalB were inhibited by RBC8 (Extended Data Fig. 8a–d) and by BQU57 (Fig. 4d) but not by the inactive compound RBC5 (Extended Data Fig. 8e, f). By contrast, no inhibition of Ras or RhoA activity was observed (Fig. 4d).

One reason for the failures to obtain clinically useful inhibitors of Ras and other related GTPases is the highly conserved guanine nucleotide binding site in these GTPases. This site has a high affinity for the guanine nucleotides GDP and GTP, which are present at millimolar concentrations in cells and would out-compete ligands for this site. Similar considerations have delayed the development of protein kinase inhibitors. Indeed some of the best kinase inhibitors have proved not to be competitive with ATP but to be allosteric inhibitors that lock the conformation of protein kinases, such as MEK, in a closed state[23]. Recently, three studies used a similar fragment-based small molecule screening approach to identify compounds that bind to sites on the K-Ras surface and block its SOS-mediated activation[24–26], suggesting that this approach has promise.

Although our initial library screening was based on the RalA structure, the selected compounds also bound to RalB, which is not surprising given the similarity of the amino acid sequences and the predicted structures. Molecular docking could not be performed on RalB–GDP since only the RalB–GNP structure is available. However, NMR experiments with RalB–GDP demonstrated interactions within the allosteric site. Moreover, the selected compounds inhibited the activity of both RalA and RalB in cell culture and in human tumour xenografts. Although RalA and RalB have been proposed to have distinct roles in tumorigenesis and metastasis[1,8,12,13], genetically engineered mouse models have revealed substantial redundancy for Ral proteins in tumorigenesis[12]. These results support the clinical utility of compounds that inhibit both of these GTPases. Although additional medicinal chemistry optimization

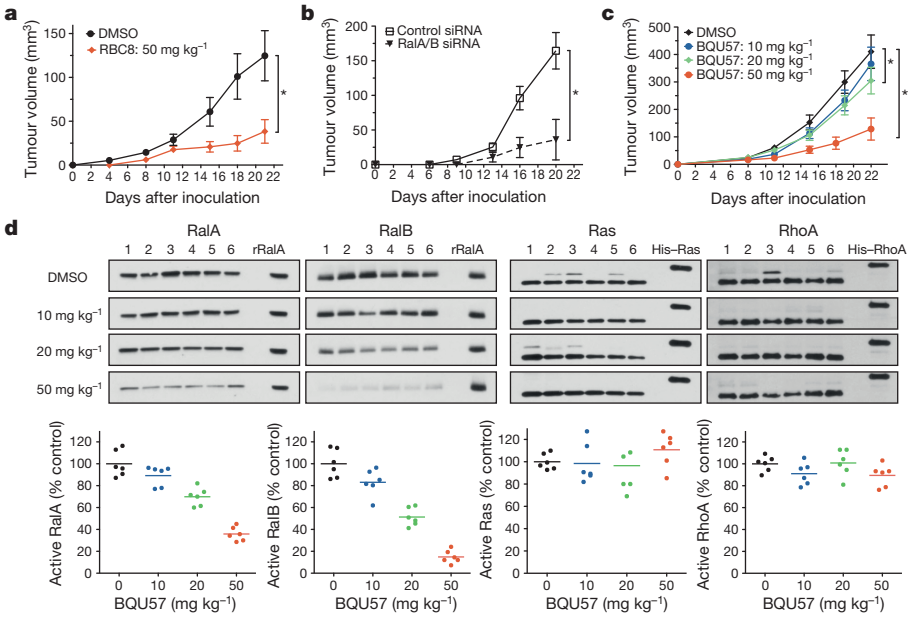

Figure 4 | Effect of Ral inhibitors *in vivo*. **a**, RBC8 (50 mg per kg body weight per day) was administered to mice 24 h after inoculation with the human lung cancer cell line H2122, and it inhibited growth of the tumour xenograft. **b**, siRNA depletion of both RalA and RalB inhibited the growth of H2122 tumour xenografts. The cells were transiently transfected with siRNA for 24 h before inoculation of nude mice. **c**, BQU57 treatment (10, 20 or 50 mg per kg body weight per day) initiated 24 h after inoculation inhibited the growth of H2122 tumour xenografts. The data in **a**–**c** are presented as the mean ± s.e.m. for groups of six mice. *, $P < 0.05$, Student's *t*-test. **d**, BQU57 treatment inhibited the activity of RalA and RalB but not Ras and RhoA in H2122 tumour xenografts. Tumour-bearing nude mice were given a single dose of 10, 20 or 50 mg per kg body weight BQU57. Tumours were collected 3 h later, and the activity of RalA, RalB, Ras and RhoA in tumour lysates was then measured using the respective pull-down assay for each GTPase. Immunoblots from the activity pull-down assays (top) and the corresponding quantifications (bottom) are shown. Each lane represents one tumour sample, and each blot represents one treatment group. The last lane in each blot was loaded with 10 ng recombinant human protein as an internal control for normalization and cross-blot comparison. The band intensity on each blot was first normalized to the internal control and then compared across different blots. The amount of active Ral, Ras or RhoA (bottom) is shown as the percentage of that in the DMSO-treated control. Each dot represents one tumour sample, and horizontal bars represent the mean of six samples. Colours match those in **c**.

is required, these Ral inhibitors represent a first generation of valuable tools for elucidating Ral signalling and for developing novel agents for cancer therapy.

Online Content Methods, along with any additional Extended Data display items and Source Data, are available in the online version of the paper; references unique to these sections appear only in the online paper.

Received 14 August 2013; accepted 24 July 2014.

Published online 14 September; corrected online 19 November 2014 (see full-text HTML version for details).

1. Lim, K. H. *et al.* Divergent roles for RalA and RalB in malignant growth of human pancreatic carcinoma cells. *Curr. Biol.* **16,** 2385–2394 (2006).
2. Schubbert, S., Shannon, K. & Bollag, G. Hyperactive Ras in developmental disorders and cancer. *Nature Rev. Cancer* **7,** 295–308 (2007).
3. Tsimberidou, A. M., Chandhasin, C. & Kurzrock, R. Farnesyltransferase inhibitors: where are we now? *Expert Opin. Investig. Drugs* **19,** 1569–1580 (2010).
4. Roberts, P. J. & Der, C. J. Targeting the Raf–MEK–ERK mitogen-activated protein kinase cascade for the treatment of cancer. *Oncogene* **26,** 3291–3310 (2007).
5. Yap, T. A. *et al.* Targeting the PI3K–AKT–mTOR pathway: progress, pitfalls, and promises. *Curr. Opin. Pharmacol.* **8,** 393–412 (2008).
6. Neel, N. F. *et al.* The RalGEF–Ral effector signaling network: the road less traveled for anti-Ras drug discovery. *Genes Cancer* **2,** 275–287 (2011).
7. Awasthi, S., Sharma, R., Singhal, S. S., Zimniak, P. & Awasthi, Y. C. RLIP76, a novel transporter catalyzing ATP-dependent efflux of xenobiotics. *Drug Metab. Dispos.* **30,** 1300–1310 (2002).
8. Oxford, G. *et al.* RalA and RalB: antagonistic relatives in cancer cell migration. *Cancer Res.* **65,** 7111–7120 (2005).
9. Lim, K. H. *et al.* Activation of RalA is critical for Ras-induced tumorigenesis of human cells. *Cancer Cell* **7,** 533–545 (2005).
10. Camonis, J. H. & White, M. A. Ral GTPases: corrupting the exocyst in cancer cells. *Trends Cell Biol.* **15,** 327–332 (2005).
11. Zipfel, P. A. *et al.* Ral activation promotes melanomagenesis. *Oncogene* **29,** 4859–4864 (2010).
12. Peschard, P. *et al.* Genetic deletion of *RALA* and *RALB* small GTPases reveals redundant functions in development and tumorigenesis. *Curr. Biol.* **22,** 2063–2068 (2012).
13. Martin, T. D. & Der, C. J. Differential involvement of RalA and RalB in colorectal cancer. *Small GTPases* **3,** 126–130 (2012).
14. Yin, J. *et al.* Activation of the RalGEF/Ral Pathway promotes prostate cancer metastasis to bone. *Mol. Cell. Biol.* **27,** 7538–7550 (2007).
15. Smith, S. C. *et al.* Expression of Ral GTPases, their effectors, and activators in human bladder cancer. *Clin. Cancer Res.* **13,** 3803–3813 (2007).
16. Smith, S. C., Baras, A. S., Owens, C. R., Dancik, G. & Theodorescu, D. Transcriptional signatures of Ral GTPase are associated with aggressive clinicopathologic characteristics in human cancer. *Cancer Res.* **72,** 3480–3491 (2012).
17. Pautsch, A., Vogelsgesang, M., Trankle, J., Herrmann, C. & Aktories, K. Crystal structure of the C3bot–RalA complex reveals a novel type of action of a bacterial exoenzyme. *EMBO J.* **24,** 3670–3680 (2005).
18. Shoichet, B. K. Virtual screening of chemical libraries. *Nature* **432,** 862–865 (2004).
19. Irwin, J. J. & Shoichet, B. K. ZINC—a free database of commercially available compounds for virtual screening. *J. Chem. Inf. Model.* **45,** 177–182 (2005).
20. Balasubramanian, N. *et al.* RalA–exocyst complex regulates integrin-dependent membrane raft exocytosis and growth signaling. *Curr. Biol.* **20,** 75–79 (2010).
21. Fenwick, R. B. *et al.* Solution structure and dynamics of the small GTPase RalB in its active conformation: significance for effector protein binding. *Biochemistry* **48,** 2192–2206 (2009).
22. Hinoi, T. *et al.* Post-translational modifications of Ras and Ral are important for the action of Ral GDP dissociation stimulator. *J. Biol. Chem.* **271,** 19710–19716 (1996).
23. Fang, Z., Grutter, C. & Rauh, D. Strategies for the selective regulation of kinases with allosteric modulators: exploiting exclusive structural features. *ACS Chem. Biol.* **8,** 58–70 (2013).
24. Sun, Q. *et al.* Discovery of small molecules that bind to K-Ras and inhibit Sos-mediated activation. *Angew. Chem. Int. Edn Engl.* **51,** 6140–6143 (2012).
25. Maurer, T. *et al.* Small-molecule ligands bind to a distinct pocket in Ras and inhibit SOS-mediated nucleotide exchange activity. *Proc. Natl Acad. Sci. USA* **109,** 5299–5304 (2012).
26. Shima, F. *et al. In silico* discovery of small-molecule Ras inhibitors that display antitumor activity by blocking the Ras-effector interaction. *Proc. Natl Acad. Sci. USA* **110,** 8182–8187 (2013).

Supplementary Information is available in the online version of the paper.

Acknowledgements This work was supported in part by NIH grants CA091846, CA075115, CA104106 and GM47214 by the IUPUI Research Scholar Grant Foundation and by an American Cancer Society Research Scholar grant. The researchers used the services of the Medicinal Chemistry Core (MCC) facility (M.F.W.) housed within the Department of Pharmaceutical Sciences, University of Colorado. In part, the MCC is funded by Colorado Clinical and Translational Sciences Institute grant UL1TR001082 from the National Center for Research Resources, NIH. We acknowledge D. S. Backos for assistance with computational modelling, A. Spencer for biochemical assays, B. Helfrich for assistance with lung cancer cell line culturing, and H. Mo and J. Harwood for assistance in the training and collection of NMR data in the early stages of the project.

Author Contributions D.T. and S.O.M. conceived of the initial screening concept. D.T. assembled the team and coordinated the project. C.Y., L.L., M.K., W.E.K., D.L., J.M., B.H., M.D.N., B.M.P., D.L.B., S.G., C.O. and C.L.W. performed experimental work and data analysis. M.F.W. performed and analysed the pharmacokinetic and pharmacodynamic experiments. D.N.M.J. performed and analysed the NMR experiments. M.A. performed GTP assays. D.T., C.Y., S.O.M., D.N.M.J., D.L.B., B.M.P., D.R. and M.A.S. wrote the manuscript.

Author Information Reprints and permissions information is available at www.nature.com/reprints. The authors declare no competing financial interests. Readers are welcome to comment on the online version of the paper. Correspondence and requests for materials should be addressed to D.T. (dan.theodorescu@ucdenver.edu).

METHODS

Materials. The human bladder cancer cell line J82 and the human lung cancer cell lines H2122, H358, H460 and Calu-6 were obtained from the ATCC. All cell lines were fingerprinted by short tandem repeat (STR) profiling and tested for mycoplasma contamination. Antibodies specific for the following proteins were used: RalA (BD Biosciences, #610222), RalB (Millipore, #04-037) and Flag tag (Novagen, #71097). siRNAs directed against human RalA and RalB or both were obtained from Dharmacon using published sequences[8]. Activity assay kits for Ras (#BK008) and RhoA (#BK036) were obtained from Cytoskeleton. All 88 Ral-binding compounds (RBCs) were purchased from ChemDiv. Unless otherwise notified, all chemicals were obtained from Sigma-Aldrich.

Computation-based molecular modelling. The crystallographic coordinates of the 2.66 Å human RalA–GDP (PDB ID, 2BOV)[27], RalA–GNP in complex with EXO84 (PDB ID, 1ZC4)[28] and RalA–GNP in complex with SEC5 (PDB ID, 1UAD)[29] crystal structures were obtained from PDB. AutoDock4 was used for the initial library screening. The ChemDiv library v2006.5 was downloaded from the ZINC database[19] and docked into the identified site on RalA–GDP using rigid docking protocols. This library includes 500,000 compounds, excluding those possessing reactive groups, known ADME toxicity and physicochemical properties that lie outside 'drug-likeness' parameters (by Lipinski's rule of five and Veber's rule of two) at pH 7. Ligand molecules were assigned Gasteiger charges and polar hydrogen atoms by the ligand preparation module provided in AutoDockTools. The Lamarckian genetic algorithm in AutoDock4 was used to evaluate ligand binding energies over the conformational search space. We then ranked compounds based on binding energy and selected top compounds for evaluation.

RalA ELISA. J82 cells stably overexpressing Flag–RalA were plated at 800,000 cells per well in 6-well plates and allowed to incubate for 16 h. Cells were treated with 500 µl fresh medium containing test compounds (50 µM) or DMSO control (1.0 h; 37 °C). Cells were then washed with ice-cold PBS and collected into ice-cold lysis buffer (750 µl containing 50 mM Tris, pH 7.5, 200 mM NaCl, 1% IGEPAL CA-630, 10 mM $MgCl_2$ and protease inhibitors). The lysate was cleared by centrifugation, and the supernatants were then flash-frozen and stored at −80 °C until testing. For the ELISA assay, HisGrab Nickel Coated 96-well plate strips (Pierce, #15142) were washed three times with ELISA buffer (200 µl consisting of 50 mM Tris, pH 8.0, 150 mM NaCl, 0.5% Tween 20, and 10 mM $MgCl_2$). RALBP1 (0.5 µg 100 μl^{-1}) was then added to the wells and incubated with rocking (2.0 h at room temperature). The plates were then washed three times with 200 µl ELISA buffer. The plates were placed on ice, and lysates, or lysis buffer control (100 µl), were added to the wells in quadruplicate. The plates were then incubated overnight with rocking at 4 °C followed by two washes with ice-cold ELISA buffer. Mouse anti-Flag antibody (Sigma, F1804; 1:20,000 in ELISA buffer) was then added at 100 µl per well and incubated (1.0 h, 4 °C). After three washes, goat anti-mouse antibody conjugated to horseradish peroxidase (HRP) (Pierce, #31430; 1:2,500) was added at 100 µl per well and incubated (1.0 h, 4 °C). HRP substrate (Vector Laboratories, #SK-4400) was added to each well at 100 µl after three washes and incubated (1.0 h, room temperature). The reactions were stopped by adding 2 M sulphuric acid (100 µl). Absorbance was read at 450 nm on a BioTek Synergy Hybrid Multi-Mode H1 plate reader (BioTek Instruments). The absorbance was corrected for background absorbance by subtracting the reading for the same well at 540 nm.

MEF spreading assay. The MEF spreading assay was performed according to published procedures[20]. Briefly, wild-type or $Cav^{-/-}$ MEFs were starved for 24 h, detached from culture plates with Accutase Cell Detachment Solution (Innovative Cell Technologies), resuspended in DMEM with 0.2% serum and 0.5% methyl cellulose, and held in suspension (90 min, 37 °C). While in suspension, cells were treated with inhibitor or DMSO for 1.0 h. After treatment, cells were rinsed once with DMEM containing 0.2% serum, and equal numbers of cells from all treatments were added to 24-well plates that had been coated overnight (4 °C) with 2.0 µg ml^{-1} human fibronectin. Cells were allowed to spread for 30 min and then fixed with formaldehyde using standard protocols. To allow visualization, cells were labelled with LavaCell (Active Motif) and visualized with a Nikon TE300 fluorescence microscope. Three distinct regions of each well were imaged, and the cell spread area was quantified using ImageJ.

NMR spectroscopy. RalB (Q72L mutant) in a pET16b plasmid (Novagen) was a gift from D. Owen. RalB was purified as previously described[21], with additional steps for loading with GDP or the non-hydrolysable form of GTP (GNP, Sigma-Aldrich), which were conducted as previously described[30]. Uniform double labelling of proteins with ^{13}C and ^{15}N was produced in M9 medium supplemented with $[^{15}N]NH_4Cl$ and [^{13}C]glucose. Samples were prepared for NMR spectroscopy in a buffer consisting of 50 mM sodium phosphate, pH 7.6, 100 mM NaCl and 1.0 mM $MgCl_2$. All NMR experiments were recorded on an Agilent 900 MHz system at 25 °C. Resonance assignments for the RalB–GNP complex were obtained from previously published studies deposited in the BMRB (ID, 15230). Chemical shift assignments of the RalB–GDP complex were obtained independently using HNCACB, CBCA(CO)NH and CCOCNH-TOCSY experiments. All NMR data were processed using NMRPipe[31] and analysed using the CcpNmr analysis program[32]. Assignments were obtained by automated assignment using PINE[33] followed by manual verification. ^{15}N-TROSY experiments were used to monitor amide shifts from the RalB protein (100 µM) following the addition of compound reconstituted in deuterated DMSO. DMSO concentrations in the final sample were 0.5% or 1%; control samples were made with 0.5% or 1% deuterated DMSO, and all samples containing compounds were compared with their corresponding DMSO control. Normalized chemical shift changes were calculated according to the equation $\Delta\delta = \sqrt{\Delta\delta H^2 + (0.15\Delta\delta N)^2}$, where $\Delta\delta H$ and $\Delta\delta N$ are the chemical shift changes for the proton and nitrogen frequencies, respectively.

ITC and SPR. ITC experiments were carried out using the MicroCal iTC200 system. RalB protein was purified, as described above. Both protein and drug were prepared in a buffer consisting of 50 mM sodium phosphate, pH 7.6, 100 mM NaCl and 1.0 mM $MgCl_2$. The final DMSO concentration was adjusted to 1%. RalB–GDP protein (300 µM) was loaded into the syringe and titrated into drug (25 µM) or buffer alone as control. All experiments were carried out at 25 °C. SPR experiments were carried out using the Biacore 3000 system. RalB protein was purified as above. The running buffer contained PBS, pH 7.4, 1.0 µM GDP, 2.0 mM $MgCl_2$ and 3% DMSO. The regeneration buffer contained PBS, pH 7.4, 1.0 µM GDP and 2.0 mM $MgCl_2$. RalB–GDP protein was immobilized onto a CM5 chip; samples of compound BQU57 in running buffer were injected at 30 µl min^{-1} for 60 s contact time followed by 5.0 min regeneration.

Guanine nucleotide binding. His–RalA (100 ng) was incubated with [γ-^{32}P]GTP (8 nM assay concentration) and either DMSO or individual compounds (50 µM assay concentration) dissolved in DMSO in the presence of EDTA (20 mM) for 15 min at 30 °C. The reaction was stopped by dilution in excess $MgCl_2$, and the incorporation of radiolabelled nucleotide was measured by filter binding[34]. [α-^{32}P]GTP was converted to [^{32}P]GDP by nucleotide diphosphokinase and used for the binding assay with GDP.

***In vitro* growth of human cancer cells.** Growth inhibition of human lung cancer cells by the compounds was measured under anchorage-independent conditions in soft agar. Cells were seeded into 6-well plates (coated with a base layer made of 2.0 ml of 1% low-melting-point agarose) at 15,000 cells per well in 3.0 ml of 0.4% low-melting-point agarose containing various concentration of drug. Two to four weeks (depending on the cell line) after incubation, the cells were stained with 1.0 mg ml^{-1} nitroblue tetrazolium, and colonies were counted under a microscope. The IC_{50} values were defined as the concentration of drug that resulted in a 50% reduction in colony number compared with the DMSO-treated control. To determine the growth effects induced by siRNA treatment, cells were transfected with 50 nM siRNA directed against *RALA*, *RALB* or both (RalA/B) using methods and sequences described previously[8]. After 48 h, cells were subjected to the soft agar colony formation assay, as described above. For the chemo-genetic experiments, siRNA-treated cells were seeded into soft agar in the presence of various concentrations of drug. For the overexpression experiments, H358 cells stably overexpressing Flag, Flag–$RalA^{G23V}$ or Flag–$RalB^{G23V}$ were generated, and cells were subjected to the soft agar colony formation assay in the presence of drug. Attempts to stably overexpress Flag–$RalA^{G23V}$ or Flag–$RalB^{G23V}$ in H2122 cells were unsuccessful, and the rescue experiments with H2122 cells were carried out 48 h after transient transfection with Flag, Flag–$RalA^{G23V}$ or Flag–$RalB^{G23V}$ using the soft agar colony formation assay in the presence of drug.

Cellular uptake and pharmacokinetic and pharmacodynamic studies. To quantify how well the compounds enter cells, H2122 human lung cancer cells were seeded at 3×10^5 cells per well in 6-well plates and incubated for 16 h. Compounds (10 µM) were individually dosed in triplicate; cells were then collected into 800 µl ice-cold 1:1:1 mixture of acetonitrile, methanol and water at different time points (1, 5, 15, 30 and 60 min). The drug concentrations in the cell lysates were then determined using the LC-MS/MS methods described below. The pharmacokinetics of RBC8 and BQU57 were determined in nude mice following a single intraperitoneal dose (50 mg per kg body weight). Blood samples were collected into EDTA-coated tubes at time intervals from 15 min to 5 h post dose (9 time points) and centrifuged at 1,500*g* for 15 min to generate plasma samples. Pharmacokinetic parameters, including the area under the curve (AUC), extrapolated initial concentration (C_o) and half-life ($T_{1/2}$), were estimated using non-compartmental methods. The pharmacodynamics of compounds were determined in tumour-bearing nude mice following a single intraperitoneal dose of 50 mg per kg body weight. Tissue samples were collected 3.0 h after the injection of RBC8 or BQU57. Tissue samples were then homogenized with two weight volumes of phosphate buffer (pH 7.4). High performance liquid chromatography (HPLC)-MS/MS methods were developed to quantify RBC8 and BQU57 in plasma and tissues. Plasma or homogenized tissue samples were extracted with a 1:1:1 mixture of acetonitrile, methanol and water, mixed and centrifuged. The supernatants were transferred into individual wells of a 96-well plate. The 96-well plate was placed into a LEAP auto-sampler (LEAP Technologies) cool stack (6.0 ± 0.1 °C)

and immediately analysed using a Shimadzu HPLC (Shimadzu Scientific Instruments) equipped with a Zorbax Extend-C18 (50 × 4.6 mm, 5 μm particle size) column (Agilent Technologies) and guard column. The mobile phase consisted of buffer A (10 mM ammonium acetate and 0.1% formic acid in water) and buffer B (a 1:1 mixture of acetonitrile and methanol). A SCIEX 4000 system (Applied Biosystems) was used for compound detection. Standard curves were prepared by spiking compounds into control plasma and tissues (for example, liver, brain, kidney, lung, heart and tumour), and these were used to determine the drug concentrations.

Tumour growth in mice. All experiments were approved by the University of Colorado Denver Animal Care and Use Committee and were carried out according to approved protocols. Female athymic nude mice (NCr *nu/nu*; National Cancer Institute) were received at 5 to 6 weeks of age and were allowed to acclimate for 2 weeks in sterile micro isolator cages with constant temperature and humidity. Mice had free access to food and water. Mice were randomized into six per group immediately before use (no blinding was done). H2122 cells in the logarithmic phase of growth were harvested on the day of use. Cells were suspended in unsupplemented RPMI 1640 medium, and 0.1 ml cells (2×10^5 cells) was injected subcutaneously at four sites per mouse. For H358 xenografts, cells (5×10^6) were mixed with Matrigel (20% final concentration), and 0.1 ml cells was inoculated subcutaneously per site. After cell inoculation, mice were monitored daily and weighed twice weekly, and caliper measurements began when the tumours became visible. Tumour volume was calculated with the equation $(L \times W^2)/2$, where L is the longer dimension of the tumour and W is the shorter dimension. Drug treatment started the day after inoculation. Compounds were dissolved in DMSO and injected intraperitoneally each day (except on weekends) at 10, 20 or 50 mg compound per kg body weight. No obvious toxicities were observed in the control (DMSO) or drug-treated animals as assessed by differences in body weight between the control and drug-treated animals taking tumour size into account.

Ral activity in tumour xenografts. Nude mice were subcutaneously inoculated with 5×10^6 H2122 cells. When the tumours reached an average of 250 mm^3, mice were randomized into six mice per group (no blinding was done) and were given an intraperitoneal dose of RBC8 or BQU57 at various concentrations. Tumours were then collected 3 h after injection of RBC8 or BQU57. The RalA and RalB activity in the tumour samples were then measured using the RALBP1 pull-down assay kit (Millipore, #14-415), as described previously[8,15]. The Ras and RhoA activity in the tumour samples were measured using the respective pull-down assay kits (Cytoskeleton, #BK008 and #BK036). All of the activity assays used western blotting as the final readout. For quantification of the immunoblots, the bands on each blot were first normalized to the respective internal control (10 ng recombinant Ral, Ras or RhoA protein in the right-most lane), and the numbers were then compared between different blots, each of which represented one treatment condition.

General statistical methods. Unless otherwise noted, the significance of the difference between control and experimental groups was tested using a two-tailed Student's *t*-test.

27. Holbourn, K. P., Sutton, J. M., Evans, H. R., Shone, C. C. & Acharya, K. R. Molecular recognition of an ADP-ribosylating *Clostridium botulinum* C3 exoenzyme by RalA GTPase. *Proc. Natl Acad. Sci. USA* **102,** 5357–5362 (2005).
28. Jin, R. *et al.* Exo84 and Sec5 are competitive regulatory Sec6/8 effectors to the RalA GTPase. *EMBO J.* **24,** 2064–2074 (2005).
29. Fukai, S., Matern, H. T., Jagath, J. R., Scheller, R. H. & Brunger, A. T. Structural basis of the interaction between RalA and Sec5, a subunit of the sec6/8 complex. *EMBO J.* **22,** 3267–3278 (2003).
30. Thompson, G., Owen, D., Chalk, P. A. & Lowe, P. N. Delineation of the Cdc42/Rac-binding domain of p21-activated kinase. *Biochemistry* **37,** 7885–7891 (1998).
31. Delaglio, F. *et al.* NMRPipe: a multidimensional spectral processing system based on UNIX pipes. *J. Biomol. NMR* **6,** 277–293 (1995).
32. Vranken, W. F. *et al.* The CCPN data model for NMR spectroscopy: development of a software pipeline. *Proteins* **59,** 687–696 (2005).
33. Bahrami, A., Assadi, A. H., Markley, J. L. & Eghbalnia, H. R. Probabilistic interaction network of evidence algorithm and its application to complete labeling of peak lists from protein NMR spectroscopy. *PLOS Comput. Biol.* **5,** e1000307 (2009).
34. Steggerda, S. M. & Paschal, B. M. The mammalian Mog1 protein is a guanine nucleotide release factor for Ran. *J. Biol. Chem.* **275,** 23175–23180 (2000).

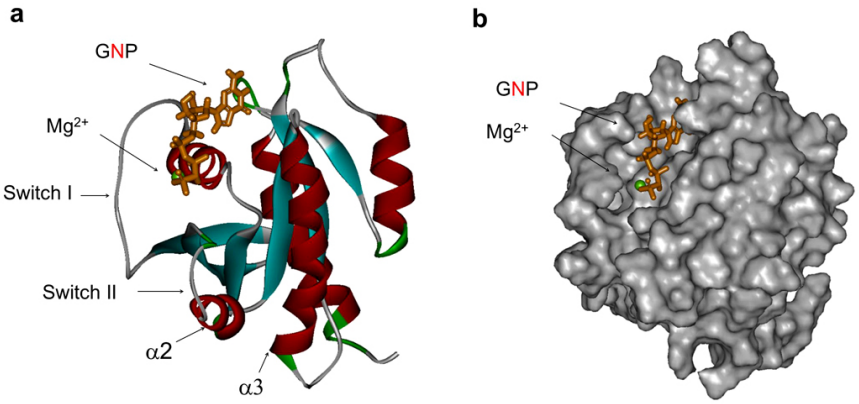

Extended Data Figure 1 | Structure model of RalB–GNP. **a**, Ribbon model showing the switch-I and switch-II regions and the α2 and α3 helices. **b**, Surface model showing absence of the allosteric binding site. All models were generated with Accelrys Discovery Studio software using the published RalB–GNP structure (PDB ID, 2KE5).

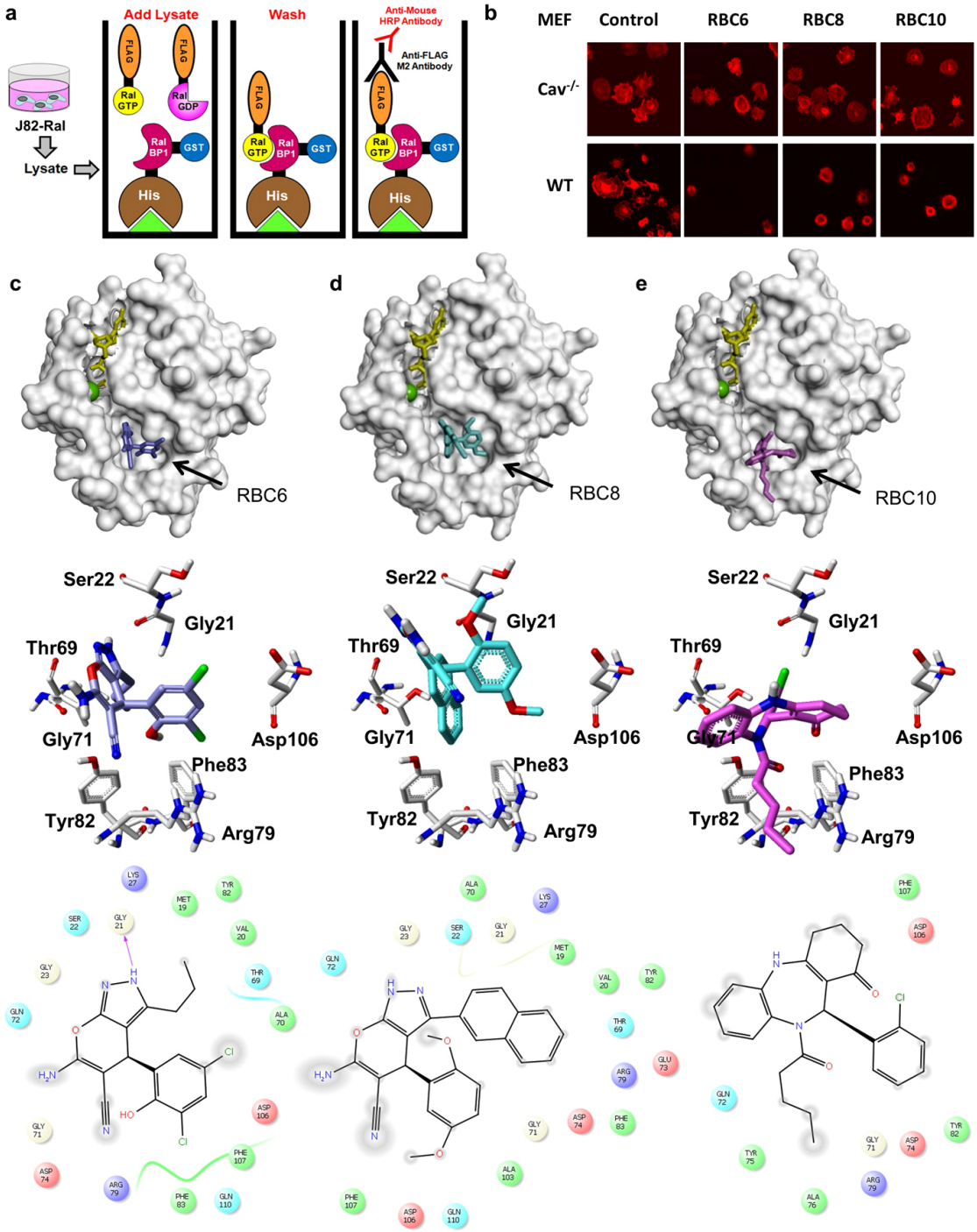

Extended Data Figure 2 | Cell-based secondary screening identified RBC6, RBC8 and RBC10 as lead compounds for Ral inhibition. **a**, Scheme for the RalA activity ELISA assay. **b**, Examples of the effects of RBC6, RBC8 and RBC10 on the RalA-dependent spreading of MEFs. Wild-type or *Cav*$^{-/-}$ MEFs were treated with 15 μM compound for 1 h and then subjected to the MEF spreading assay, as described in Methods. **c**–**e**, Molecular docking of RBC6 (**c**), RBC8 (**d**) and RBC10 (**e**) into the target site of RalA–GDP. Compounds are shown in stick form and coloured purple (RBC6), cyan (RBC8) and pink (RBC10).

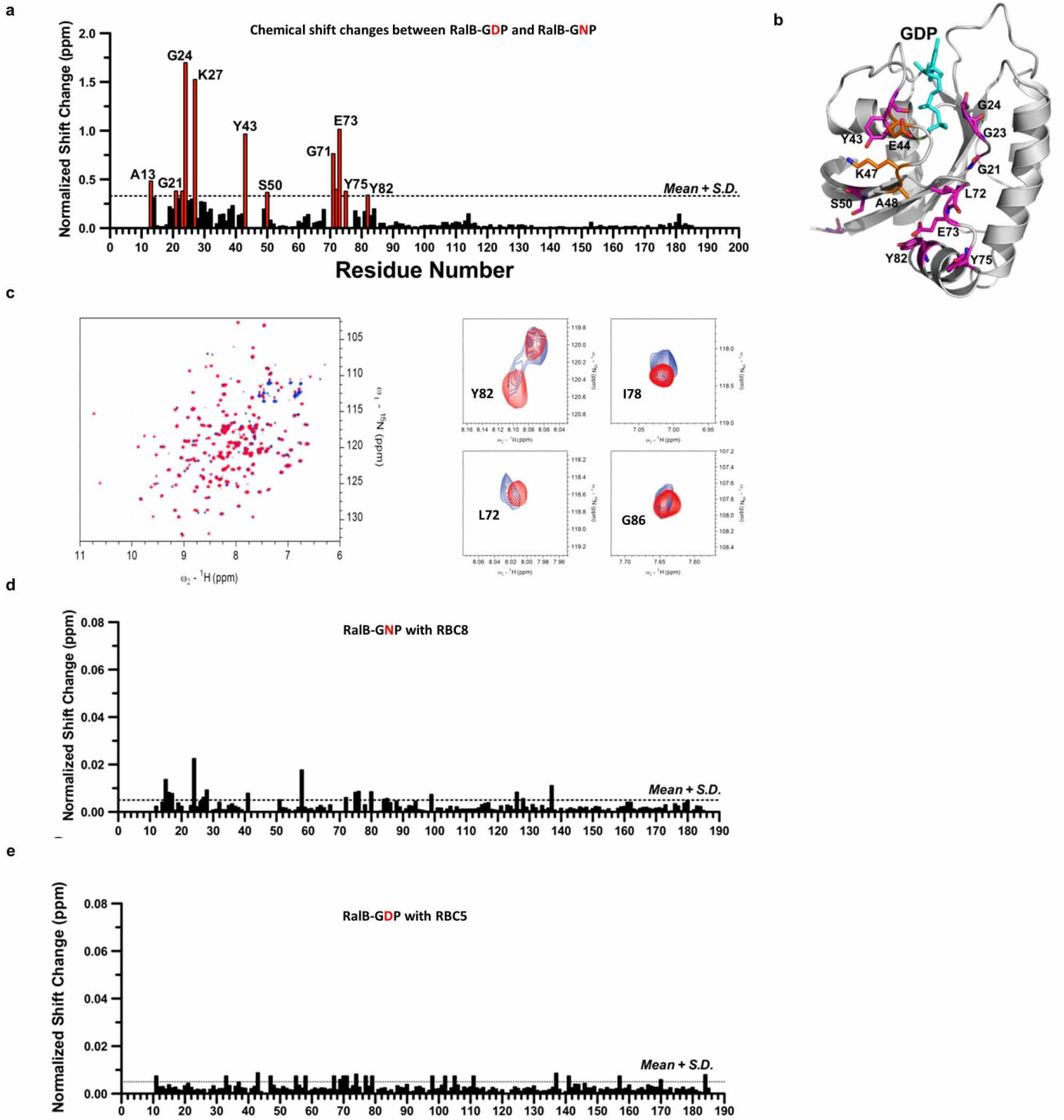

Extended Data Figure 3 | NMR characterization of compound binding to Ral. a, Plot of chemical shift differences between RalB–GDP and the previously published RalB–GNP structure (PDB ID, 2KE5) as a function of residue number. **b**, Mapping of chemical shift changes onto a homology model of the RalB–GDP complex (the model is based on RalA–GDP; PDB ID, 1U90). The mapping reveals that changes (magenta) mostly result from changes in the two loops that would otherwise bind to the third phosphate of GTP. GDP is shown as a stick model in cyan. **c**, ^{15}N-TROSY spectrum of RalB–GDP (100 μM) in the absence (red) and presence (blue) of RBC8 (100 μM). Selected residues exhibiting significant chemical shift changes are also shown. **d**, Chemical shift changes in the RalB–GNP spectrum in the presence of RBC8 (100 μM). **e**, Chemical shift changes in the RalB–GDP (100 μM) spectrum in the presence of RBC5 (100 μM).

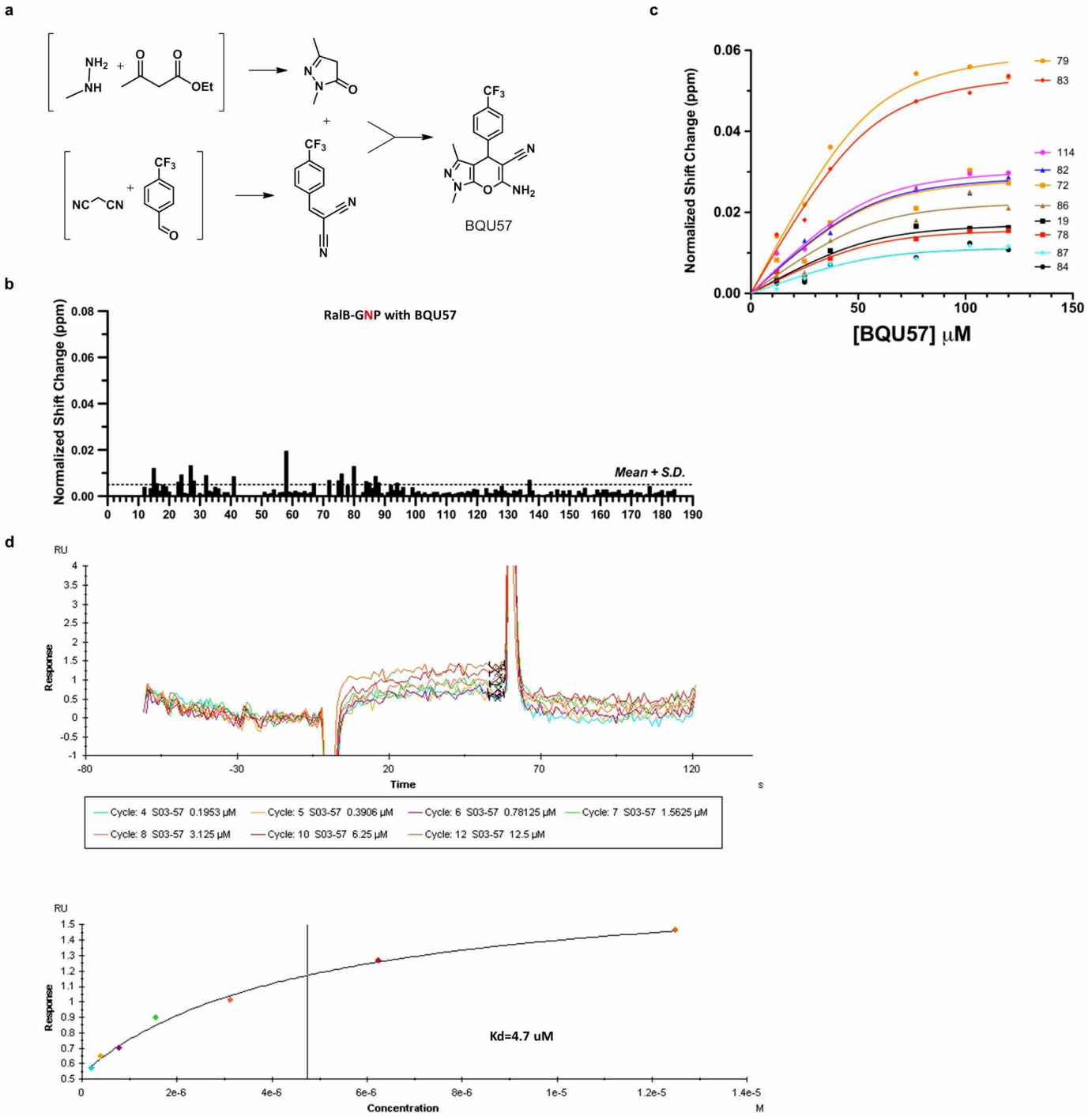

Extended Data Figure 4 | Characterization of BQU57 binding to Ral. **a**, Scheme for the chemical synthesis of BQU57. **b**, Chemical shift changes in RalB–GNP (100 μM) in the presence of BQU57 (100 μM). **c**, Plot of the ^{1}H–^{15}N-TROSY NMR chemical shift changes of selected residues in RalB–GDP with increasing concentrations of BQU57. **d**, Determination of the K_d for the binding of BQU57 to RalB–GDP using SPR. Top, SPR spectrum with increasing concentrations of BQU57; bottom, fitted binding curve, yielding a K_d of 4.7 μM.

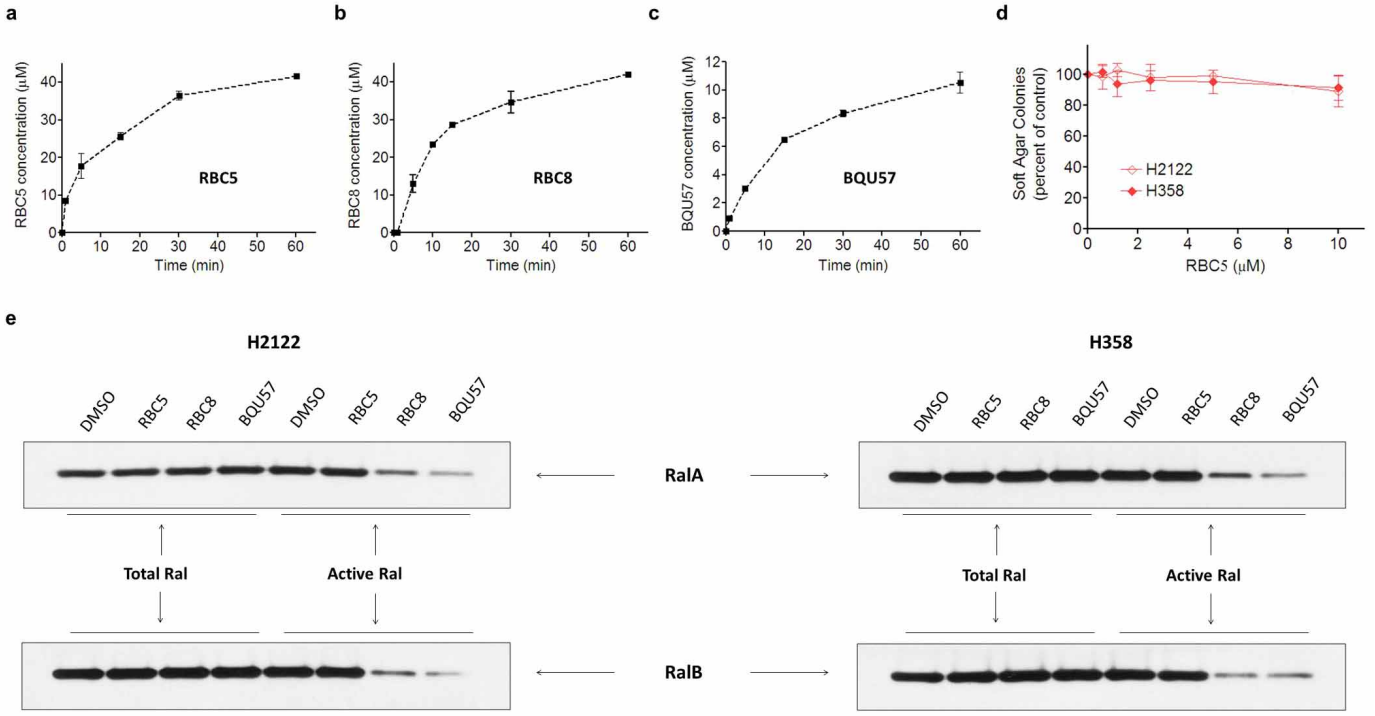

Extended Data Figure 5 | Activity of Ral inhibitors on human cancer cell lines *in vitro*. **a**–**c**, Cellular uptake of Ral inhibitors *in vitro*. H2122 human lung cancer cells were treated with RBC5, RBC8 or BQU57 (10 μM). The cells were collected at various time points (1, 5, 15, 30 and 60 min), and the drug concentrations in cells were determined using LC-MS/MS methods. The data are presented as the mean ± s.d. of triplicate samples. **d**, Effect of RBC5 treatment on the anchorage-independent growth of H2122 and H358 human lung cancer cell lines. The cells were seeded in soft agar containing various concentrations of each drug; the colonies that formed in soft agar were counted after 2–4 weeks. The data are presented as the mean ± s.d. of triplicate samples. **e**, Inhibition of Ral activity in H2122 and H358 cells by RBC5, RBC8 and BQU57. The cells were grown under anchorage-independent conditions and treated with 10 μM compound for 3 h. The Ral activity in cell lysates was then determined using a pull-down assay with RALBP1–agarose beads. Total lysates (20 μg protein) and RALBP1 pull-downs (from 400 μg protein) were analysed by immunoblotting using antibodies specific for RalA and RalB. The data represent three independent experiments.

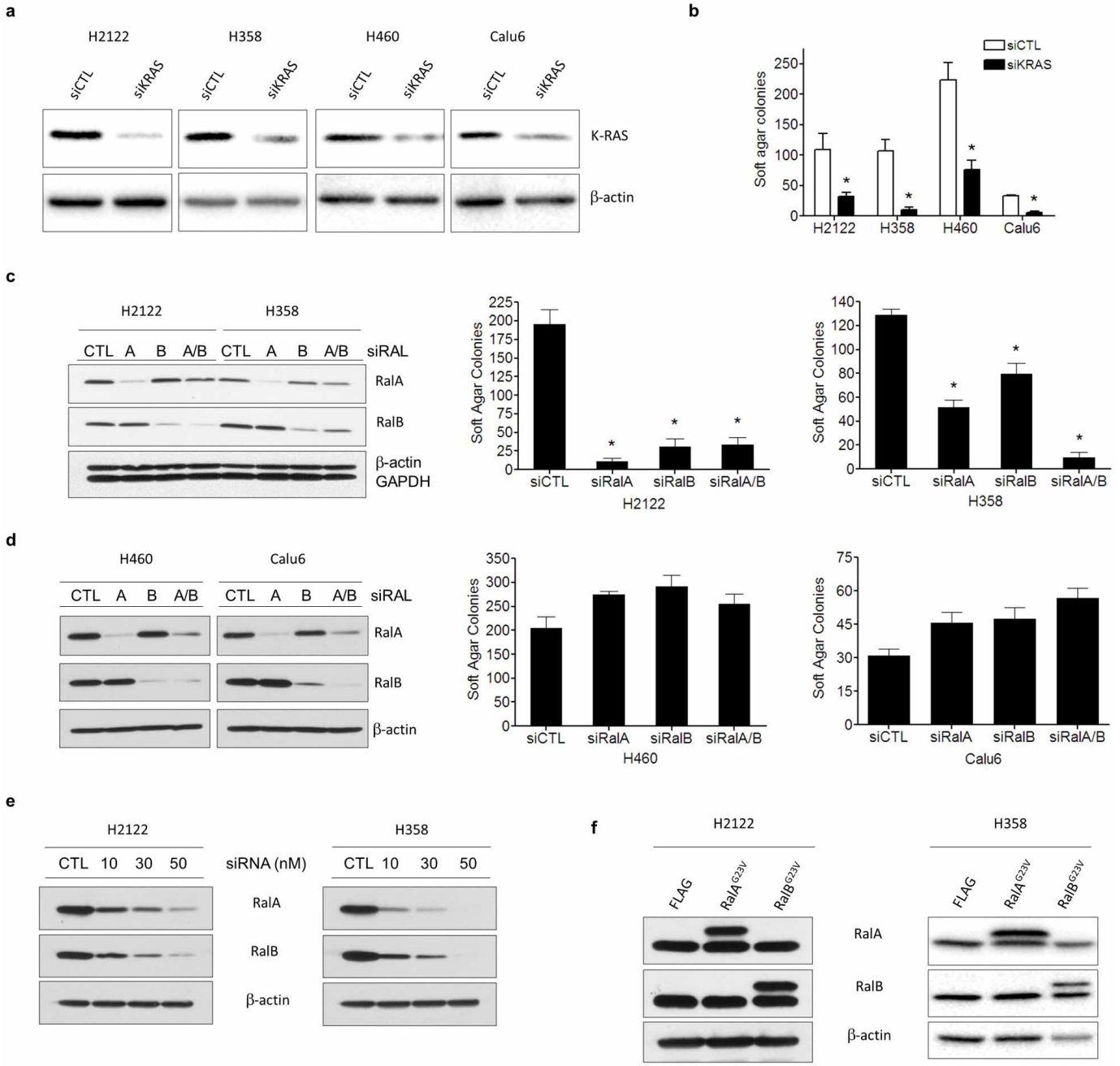

Extended Data Figure 6 | *RAS* and *RAL* knockdown in human cancer cell lines. **a**, **b**, Effect of K-*RAS* knockdown on anchorage-independent growth of four human lung cancer cell lines. Immunoblot showing siRNA-mediated knockdown of K-*RAS* in H2122, H358, H460 and Calu-6 cell lines 48 h after siRNA transfection (**a**). All four cell lines were sensitive to K-*RAS* knockdown, as determined using the soft agar colony formation assay (**b**). The data are presented as the mean ± s.d. of triplicate samples. *, $P < 0.05$, Student's *t*-test. **c**, **d**, Effect of *RAL* knockdown on anchorage-independent growth of four human lung cancer cell lines. The cells were transfected with siRNA directed against *RALA*, *RALB* or *RALA* and *RALB* (RalA/B) for 48 h and then subjected to the soft agar colony formation assay. H2122 and H358 (**c**) but not H460 or Calu-6 (**d**) were sensitive to *RAL* knockdown. The data are presented as the mean ± s.d. of triplicate samples. *, $P < 0.05$, Dunnett's test. **e**, Immunoblots showing knockdown of both *RALA* and *RALB* in H2122 and H358 cell lines 48 h after treatment with various concentrations of siRNA. **f**, Immunoblots showing successful overexpression of constitutively active $RalA^{G23V}$ or $RalB^{G23V}$ in H2122 and H358 cells. H2122 cells were transiently transfected with Flag, Flag–$RalA^{G23V}$ or Flag–$RalB^{G23V}$ for 48 h. H358 cells stably overexpressing Flag, Flag–$RalA^{G23V}$ and Flag–$RalB^{G23V}$ were generated by selection on the antibiotic G418.

a

	RBC8	BQU57
Dose (mg/kg) i.p.; n=3	50.0	50.0
Co (μM)	41.2 ± 4.2	41.6 ± 5.1
$T_{1/2}$ (hr)	0.58 ± 0.26	1.50 ± 0.11
$AUC_{0\text{-}5hr}$ (μg • h / mL)	139.6 ± 18.8	28.6 ± 2.1

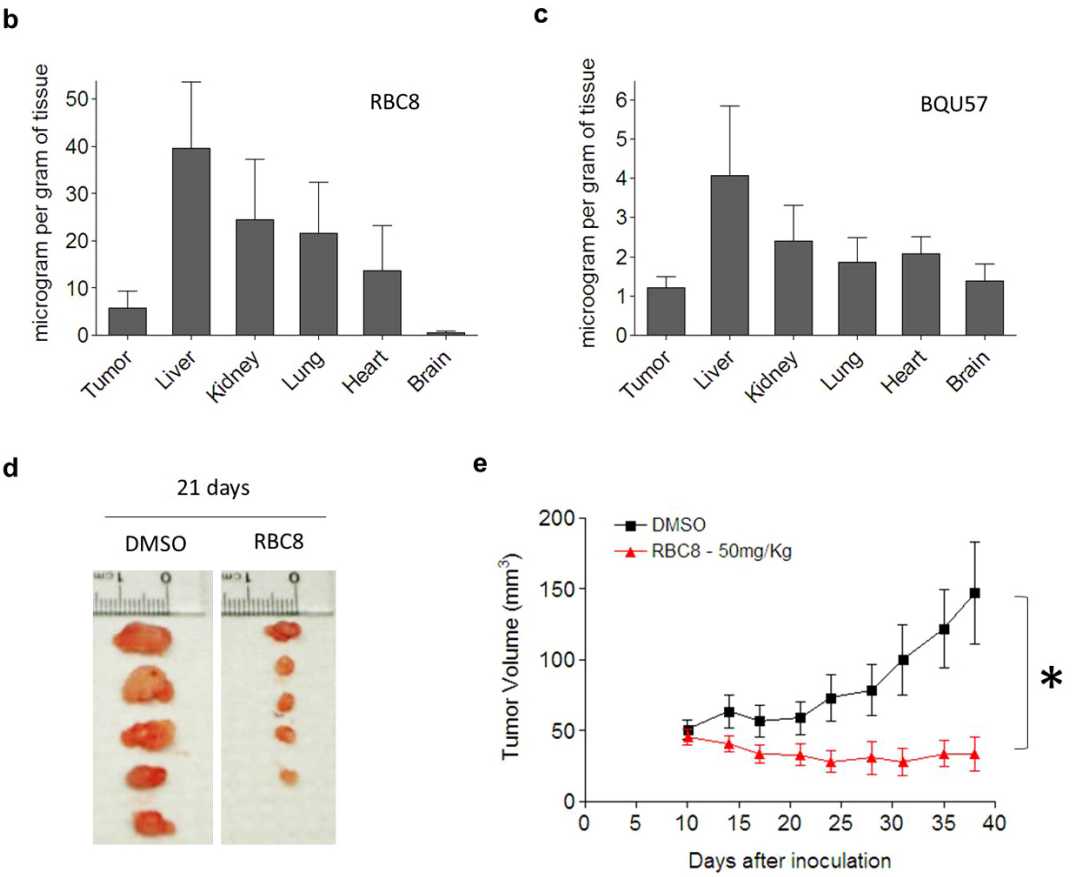

Extended Data Figure 7 | Effect of Ral inhibitors on xenograft models of human lung cancer. **a**, Summary of the pharmacokinetic parameters of RBC8 and BQU57 in nude mice. Pharmacokinetic parameters were measured based on plasma levels after administration of a single intraperitoneal dose of 50 mg Ral inhibitor per kg body weight. $AUC_{0-5\,h}$, area under the curve, 0 to 5 h; C_o, extrapolated initial concentration; $T_{1/2}$, half-life. **b**, **c**, Tissue distribution of RBC8 (**b**) and BQU57 (**c**) in nude mice 3 h after a single intraperitoneal dose of 50 mg Ral inhibitor per kg body weight. The data are presented as the mean ± s.d. for three mice. **d**, RBC8 (50 mg per kg body weight per day), initiated 24 h after inoculation, inhibited the growth of tumour xenografts of the human lung cancer cell line H2122. Typical tumour appearance at 21 days is shown. **e**, Effect of RBC8 on H358 xenograft models. RBC8 treatment (50 mg per kg body weight per day), initiated 24 h after inoculation, inhibited the growth of tumour xenografts of the human lung cancer cell line H358. The data are presented as the mean ± s.e.m. for six mice. The tumour volume in the treatment group was significantly different from that in the control group, as determined by Student's *t*-test (*, $P < 0.05$).

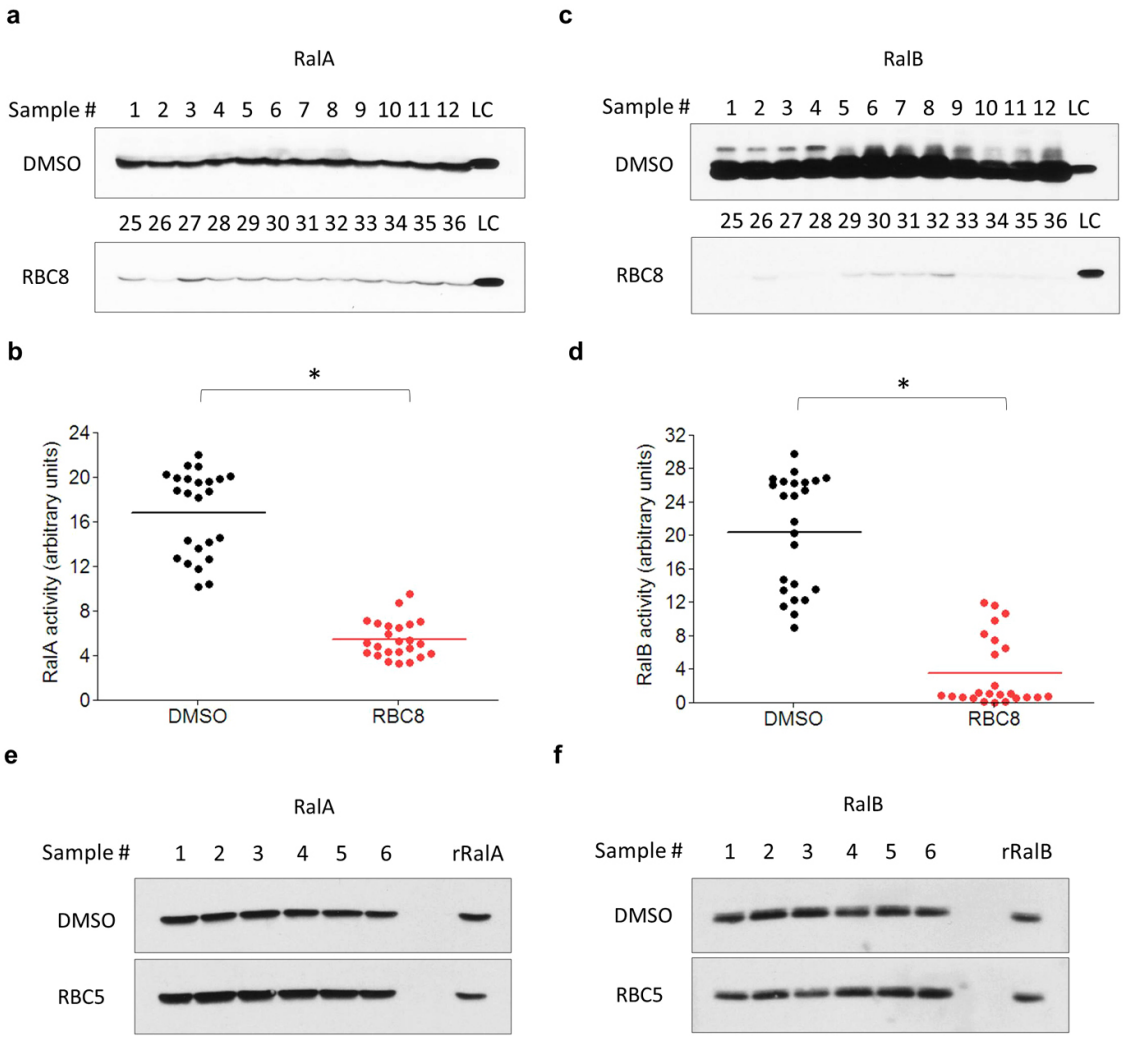

Extended Data Figure 8 | Inhibition of Ral activity by RBC8 and RBC5 *in vivo*. **a**–**d**, RBC8 inhibited RalA (**a**, **b**) and RalB (**c**, **d**) activity in H2122 tumour xenografts. Tumour-bearing nude mice were given a single dose of 50 mg RBC8 per kg body weight. After 3 h, the tumours were collected, and the Ral activity in tumour lysates was measured using the RALBP1 pull-down assay. Immunoblots from the Ral activity pull-down assay (**a**, **c**) and their quantification (**b**, **d**) are shown. Each lane represents one tumour sample. Each blot represents one treatment. The last lane in each blot (labelled LC, loading control) was loaded with 10 ng recombinant human RalA or RalB as an internal control for normalization and cross-blot comparison. The band intensity on each blot was first normalized to the internal control and then compared across different blots. The Ral activities in the treatment groups were significantly different from those in the controls, as determined by Student's *t*-test (*, $P < 0.001$, $n = 24$). **e**, **f**, RBC5 did not inhibit RalA (**e**) or RalB (**f**) activity in H2122 tumour xenografts. Tumour-bearing nude mice were given a single dose of 50 mg RBC5 per kg body weight. After 3 h, the tumours were collected, and the Ral activity in tumour lysates was measured using the RALBP1 pull-down assay ($n = 6$).